Macromolecules

Article

Cite This: *Macromolecules* 2018, 51, 6451−6459

pubs.acs.org/Macromolecules

Hydrogen-Bonding Strength Influences Hierarchical Self-Assembled Structures in Unusual Miscible/Immiscible Diblock Copolymer Blends

Tzu-Chun Tseng and Shiao-Wei Kuo*

Department of Materials and Optoelectronic Science, National Sun Yat-Sen University, Kaohsiung 80424, Taiwan

Supporting Information

ABSTRACT: We used sequential anionic living polymerization to synthesize poly(styrene-*b*-4-vinylpyridine) (PS-*b*-P4VP) and poly(vinylphenol-*b*-methyl methacrylate) (PVPh-*b*-PMMA) diblock copolymers presenting various hydrogen bond donor or acceptor units. Upon blending with the miscible disordered PVPh-*b*-PMMA diblock copolymers, we observed order−order morphological transitions from the bicontinuous gyroid structure of pure PS-*b*-P4VP to lamellar, cylindrical, and worm-like structures, in a manner strongly dependent on the concentration and vinylphenol content of the PVPh-*b*-PMMA diblock copolymer. We took advantage of competitive hydrogen-bonding interactions and ΔK effects between PVPh/P4VP and PVPh/PMMA domains when blending immiscible A-*b*-B diblock copolymers with disordered miscible C-*b*-D diblock copolymers to form hierarchical self-assembled nanostructures, including three-phase lamellar and core−shell cylindrical nanostructures.

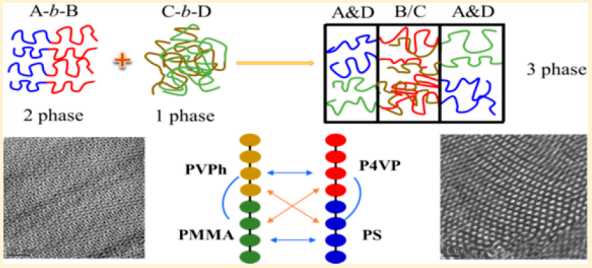

INTRODUCTION

The self-assembly of diblock copolymers (A-*b*-B) into, for example, lamellar, cylinder, double-gyroid, and spherical nanostructures has possible applications in nanotechnology, photonic crystals, and drug delivery.[1−4] Nevertheless, controlling the volume fractions of the blocks with different molecular weights through living polymerization can be complicated and time-consuming; accordingly, blending a homopolymer C into a diblock copolymer, with stabilization through hydrogen bonding, has become a preferred method for varying volume fractions and, thereby, preparing well-defined self-assembled nanostructures.[5−7] Four different systems have been reported, either theoretically or experimentally, for such A-*b*-B/C blends featuring hydrogen-bonding interactions.[8−25] In general, only typical self-assembled structures (e.g., lamellar, cylinder, double-gyroid, and spherical nanostructures) have been observed from the microphase separation of diblock copolymers in A-*b*-B/C blends, forming so-called two-phase systems (Scheme 1a). For example, the structures formed from poly(styrene-*b*-vinylphenol) (PS-*b*-PVPh) blended with polyvinylpyrrolidone (PVP), poly(4-vinylpyridine) (P4VP), poly(2-vinylpyridine) (P2VP), polycaprolactone (PCL), and poly(methyl methacrylate) (PMMA) homopolymers;[7,11−13] poly(isoprene-*b*-2-vinylpyridine) (PI-*b*-P2VP), PS-*b*-P2VP, and PS-*b*-P4VP blended with phenolic[8] and PVPh homopolymers;[9,10] PCL-*b*-P2VP and PCL-*b*-P4VP diblock copolymers blended with PVPh, phenolic, and phenoxy homopolymers;[14−21] and PVPh-*b*-PMMA and PVPh-*b*-PCL blended with PVP homopolymers[32,33] have all been reported from experimental observations.[23,25]

Scheme 1. Cartoon Representations of the Self-Assembled Structures Formed from (a) A-*b*-B/C (Two-Phase + One-Phase Becomes Two-Phase), (b) A-*b*-B/C-*b*-D (Two-Phase + Two-Phase Becomes Three-Phase), and (c) (b) A-*b*-B/C-*b*-D (Two-Phase + One-Phase Becomes Three-Phase) Blends

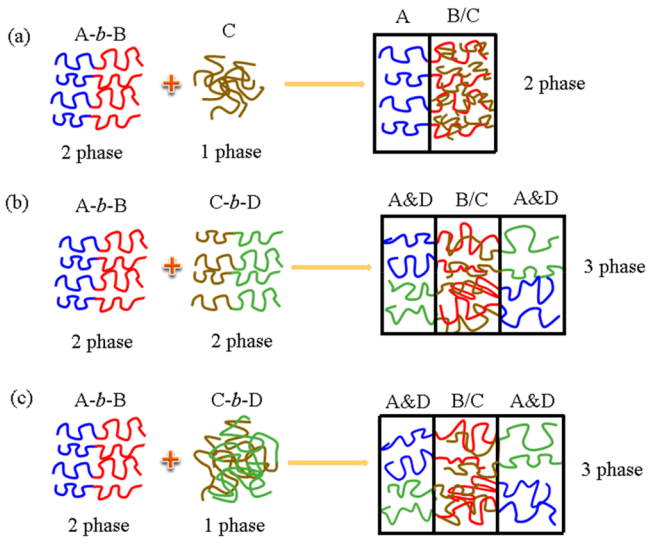

Received: April 9, 2018
Revised: July 31, 2018
Published: August 15, 2018

DOI: 10.1021/acs.macromol.8b00751
Macromolecules 2018, 51, 6451−6459

Scheme 2. Synthesis of (a) PS-*b*-P4VP and (b) PVPh-*b*-PMMA Diblock Copolymers through Sequential Anionic Living Polymerizations

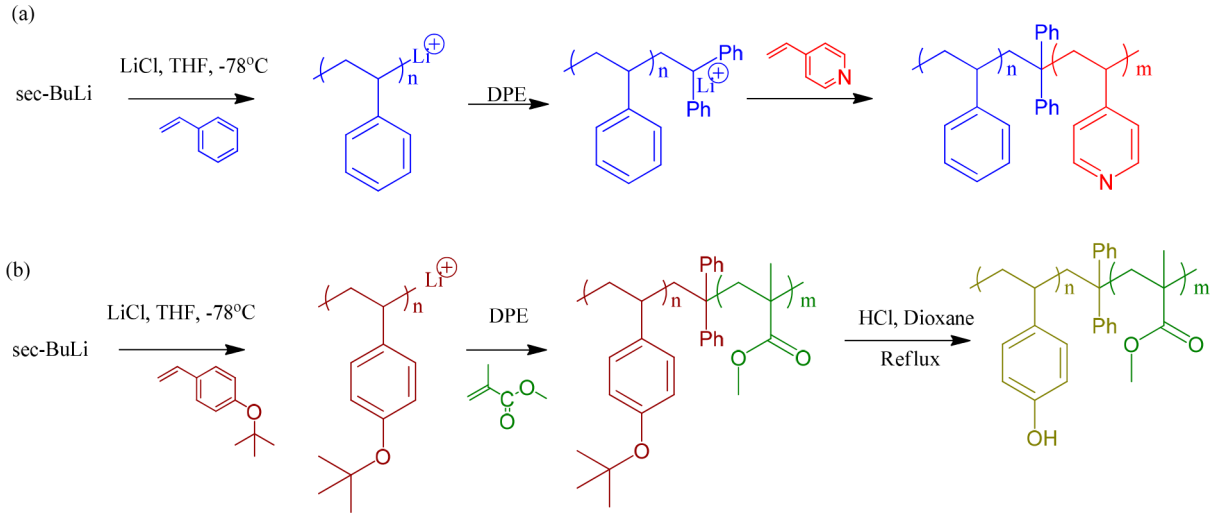

In addition to the A-*b*-B diblock copolymers that form only a few self-assembled nanostructures, the various hierarchical self-assembled structures (e.g., three-phase lamellar or core−shell cylindrical structures) formed from A-*b*-B-*b*-C triblock copolymers have also received significant interest recently.[26,27] Nevertheless, the synthesis of A-*b*-B-*b*-C triblock copolymers is even more difficult and complicated than that of diblock copolymers. As a result, the blending of A-*b*-B and C-*b*-D diblock copolymers, where the B and C block segments are capable of intermolecular hydrogen bonding, while the A and D block segments are relatively immiscible, has become a simpler approach for the preparation of such hierarchical self-assembled nanostructures, in a so-called three-phase system (Scheme 1b).[26−29] For instance, when blending PS-*b*-PVPh with P4VP-*b*-PMMA and P4VP-*b*-PCL diblock copolymers, we have observed three-phase nanostructures both in solution and in the solid state.[30−34] Furthermore, Matsushita et al. investigated the blending of PS-*b*-PVPh and PI-*b*-P2VP diblock copolymers and obtained hierarchical self-assembled structures, including lamellar-within-lamellar and cylinder-within-lamellar nanostructures.[28] Tang et al. also reported the blending of PEO-*b*-(PS-*r*-PVPh) with (PS-*r*-P4VP)-*b*-PMMA and the formation of critical cylindrical domains.[35]

On the basis of these results, we suspected that the blending of an immiscible A-*b*-B diblock copolymer (two phases arising from microphase separation of the diblock copolymer) with a homopolymer C (disordered single phase), where the B and C block segments are miscible through intermolecular hydrogen bonding, should form only a two-phase system featuring typical self-assembled nanostructures (i.e., a two-phase system plus a one-phase system becomes a two-phase system), as displayed in Scheme 1a. Furthermore, the blending of an immiscible A-*b*-B diblock copolymer with an immiscible C-*b*-D diblock copolymer (where the B and C segments are miscible through intermolecular hydrogen bonding, while the A and D segments are immiscible) should form hierarchical self-assembled nanostructures (a two-phase system plus a two-phase system becomes a three-phase system), as displayed in Scheme 1b. Here, we report the blending of immiscible A-*b*-B diblock copolymers with disordered miscible C-*b*-D diblock copolymers to form hierarchical self-assembled nanostructures (i.e., two-phase system plus a one-phase system forming a three-phase system), as displayed in Scheme 1c. In this study, we use the immiscible PS-*b*-P4VP diblock copolymers with miscible PVPh-*b*-PMMA diblock copolymers that also provide hierarchical self-assembled nanostructures, including three lamellar and core−shell cylinder nanostructures. We describe the competitive hydrogen bonding, miscibility, and hierarchical self-assembled nanostructures formed in these systems.

EXPERIMENTAL SECTION

Materials. Styrene (Aldrich, 99%), 4-vinylpyridine (Aldrich, 99%), 4-*tert*-butoxystyrene (tBOS, Aldrich, 99%), and MMA (SHOWA, 99%) monomers were distilled from CaH_2 prior to use. *sec*-Butyllithium (Acros, 1.3 M in cyclohexane) was used as an initiator for anionic living polymerization. PS_{263}-*b*-$P4VP_{106}$ (M_n = 38600 g/mol, PDI = 1.04) was synthesized through sequential anionic living polymerization, as displayed in Scheme 2a and described elsewhere.[36,37] PVPh-*b*-PMMA copolymers featuring various PVPh volume fractions were also prepared through sequential anionic living polymerizations from the monomers tBOS and MMA.[38] The *tert*-butoxy protective units of these PtBOS-*b*-PMMA block copolymers were removed through hydrolysis to form PVPh-*b*-PMMA block copolymers, as described previously (Scheme 2b).[38] The molecular weights, polydispersities, and glass transition temperatures of these diblock copolymers are summarized in Table 1.

Table 1. Molecular Weights and Glass Transition Temperatures of PS-*b*-P4VP and PVPh-*b*-PMMA Diblock Copolymers Synthesized in This Study

block copolymer	M_n (g/mol)	M_w/M_n	T_g (°C)
$PVPh_{20}$-*b*-$PMMA_{176}$	20000	1.15	137
$PVPh_{40}$-*b*-$PMMA_{112}$	16000	1.11	148
$PVPh_{137}$-*b*-$PMMA_{135}$	30000	1.10	168
$PVPh_{137}$-*b*-$PMMA_{55}$	22000	1.13	181
PS_{263}-*b*-$P4VP_{106}$	38600	1.04	108/154

PS-*b*-P4VP/PVPh-*b*-PMMA Diblock Copolymer Mixtures. Mixtures of various PS-*b*-P4VP/PVPh-*b*-PMMA compositions were prepared through solution blending. The diblock copolymers were dissolved (5 wt %) in DMF, a common solvent for all of the four block segments. The mixtures of diblock copolymer were stirred for 24 h at room temperature and then cast on an aluminum disk. The DMF was evaporated slowly at 90 °C over 2 days; the samples were

DOI: 10.1021/acs.macromol.8b00751
Macromolecules 2018, 51, 6451−6459

then dried under vacuum at 130 °C for 5 days to remove residual DMF.

Characterization. Fourier transform infrared (FTIR) spectra of the diblock copolymer mixtures were recorded using the conventional KBr disk method and a Bruker Tensor 27 FTIR spectrophotometer (32 scans; spectral resolution: 4 cm^{-1}). Thermal analyses were performed using a TA Q-20 instrument operated at a heating rate of 20 °C min^{-1} from 30 to 250 °C. Small-angle X-ray spectroscopy (SAXS) was performed using the BL23A1 (λ = 1.1273 Å) beamline at the National Synchrotron Radiation Research Center (NSRRC), Taiwan; the blend samples were sealed between Kapton windows, and their spectra were recorded at room temperature. Transmission electron microscopy (TEM) images of the diblock copolymer mixtures were recorded using a JEOL 2100 microscope operated at 200 kV. The films of the diblock copolymer mixture were cut into ultrathin sections using a Leica ultracut microtome featuring a diamond knife. TEM images were recorded after staining with I_2 (to display the P4VP block domains) and RuO_4 (to observe the PVPh block domains). Accordingly, the PVPh/P4VP complex domains appeared dark, the PMMA domains appeared gray, and the PS domains appeared white.

RESULTS AND DISCUSSION

FTIR Spectroscopic Analyses of PS-*b*-P4VP/PVPh-*b*-PMMA Diblock Copolymer Mixtures. We synthesize two different diblock copolymers presenting hydrogen bond donor or acceptor units through sequential anionic living polymerization (Scheme 2). The interaction parameter, interassociation equilibrium constant, molecular weight, molecular volume, and solubility parameter of each block segment are summarized in Scheme 3 and Table 2. In total, six different interaction parameters existed for these PS-*b*-P4VP/PVPh-*b*-PMMA diblock copolymer mixtures; as displayed in Scheme 3, four of the interaction parameters were positive, suggesting that the PS/P4VP, PS/PVPh, PS/PMMA, and P4VP/PMMA binary blend systems were immiscible or phase-separated. Furthermore, two of the interaction parameters were negative: those for miscible PVPh/P4VP and PVPh/PMMA binary blends. Nevertheless, the interassociation equilibrium constant of the PVPh/P4VP binary blend (K_A = 1200)[39,40] is significantly higher than that of the PVPh-*b*-PMMA diblock copolymer (K_A = 47),[38] implying that the OH units of PVPh would prefer to interact with the pyridine units of P4VP rather than the C═O units of PMMA. As a result, the PMMA block segments might undergo microphase separation from miscible PVPh-*b*-PMMA diblock copolymers when blending with PS-*b*-P4VP diblock copolymers, thereby inducing hierarchical self-assembled nanostructures.

Scheme 3. Interaction Parameters and Interassociation Equilibrium Constants for Mixtures of PS-*b*-P4VP and PVPh-*b*-PMMA Diblock Copolymers

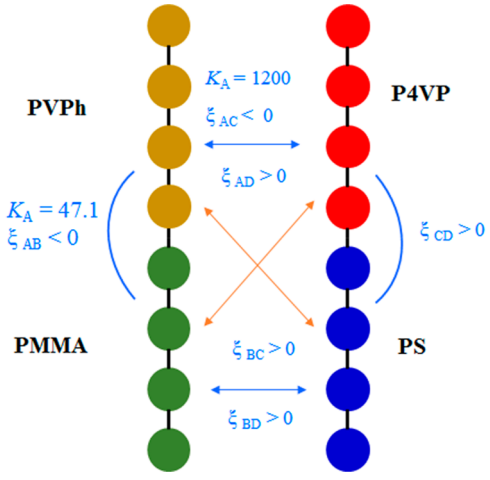

Figure 1 displays the FTIR spectra of various PS-*b*-P4VP/PVPh-*b*-PMMA diblock copolymer mixtures at room temperature, in the range from 1760 to 1680 cm^{-1} for the C═O stretching vibrations of the PMMA block segment. For the pure PVPh-*b*-PMMA diblock copolymers, two absorption peaks appeared at 1705 and 1730 cm^{-1}, representing the hydrogen-bonded and free C═O units, respectively; they could be fitted well by Gaussian functions. A higher fraction of hydrogen-bonded C═O units arose when the content of vinylphenol units was higher in the PVPh-*b*-PMMA diblock copolymers, as expected. The fraction of hydrogen-bonded C═O units of the PMMA block segments in all of the miscible PVPh-*b*-PMMA diblock copolymers decreased significantly upon increasing the concentration of the PS-*b*-P4VP diblock copolymer.

Figure 2 displays FITR spectra (from 1020 to 980 cm^{-1}) revealing the signals of the pyridine units in the P4VP block segments of various PS-*b*-P4VP/PVPh-*b*-PMMA diblock copolymer mixtures at room temperature. The characteristic peak at 993 cm^{-1} corresponds to the free pyridyl ring; a new band appeared at 1005 cm^{-1} after blending with the PVPh-*b*-PMMA diblock copolymers, representing the pyridyl rings hydrogen-bonded with the OH units of the PVPh block segments. Again, these two peaks were fitted well to Gaussian functions. At the same PS-*b*-P4VP/PVPh-*b*-PMMA blend ratio, the fraction of hydrogen-bonded pyridine rings also increased upon increasing the content of vinylphenol units in the PVPh-*b*-PMMA diblock copolymers. Figure 3A reveals that the fractions of the hydrogen-bonded C═O units of PMMA decreased upon increasing the concentration of PS-*b*-P4VP, and Figure 3B reveals that the fractions of the hydrogen-bonded pyridine units of P4VP increased upon increasing the concentration of PVPh-*b*-PMMA as would be expected. Most

Table 2. Molecular Weights, Molecular Volumes, Solubility Parameters, Equilibrium Constants, and Electron Density of the Polymers Used in This Study

polymer	molar volume (mL/mol)	molecular weight (g/mol)	solubility parameter $[(cal/mL)^{1/2}]$	equilibrium constants[a] K_2	K_B	K_A	scattering length density $(10^{-6}/Å^2)$
PVPh	82.3	120.1	11.0	21.0	66.8		10.520
PMMA	84.9	100.0	9.1			47.1	10.841
P4VP	84.9	105.1	10.8			1200	10.063
PS	93.9	104.1	9.5				9.516

[a]Self-association equilibrium constants: K_2 (dimer) and K_B (multimer); interassociation equilibrium constant: K_A.

DOI: 10.1021/acs.macromol.8b00751
Macromolecules 2018, 51, 6451−6459

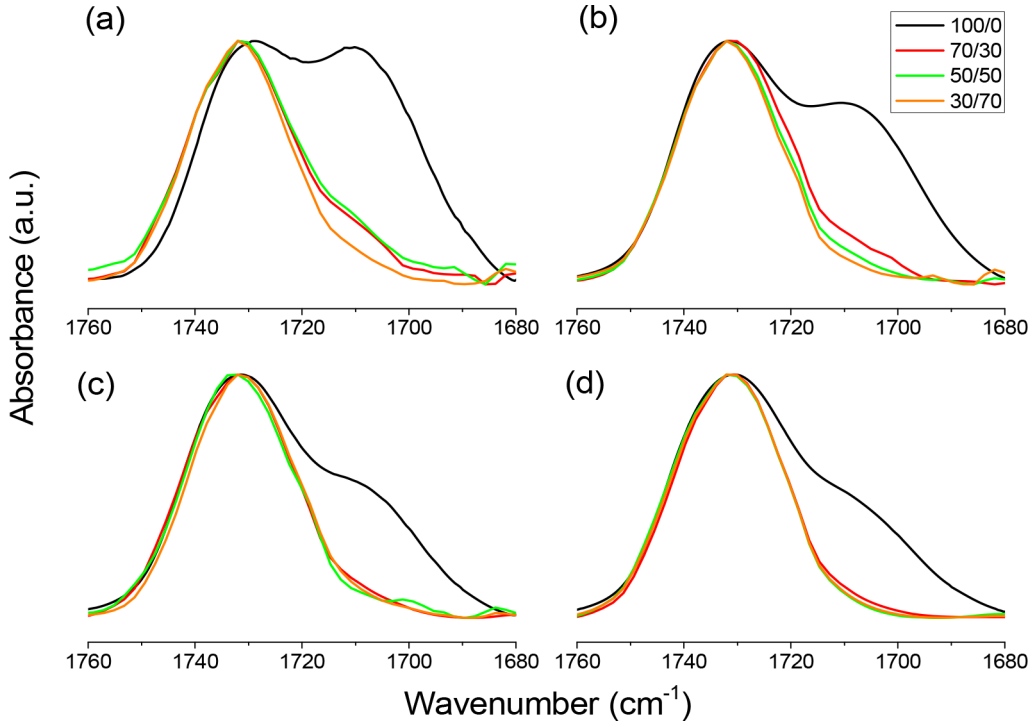

Figure 1. FTIR spectra (C═O stretching region, 1760−1680 cm^{-1}), recorded at room temperature, of (a) $PVPh_{137}$-*b*-$PMMA_{55}$, (b) $PVPh_{137}$-*b*-$PMMA_{135}$, (c) $PVPh_{40}$-*b*-$PMMA_{112}$, and (d) $PVPh_{20}$-*b*-$PMMA_{176}$ in the presence of various amounts of the diblock copolymer PS-*b*-P4VP.

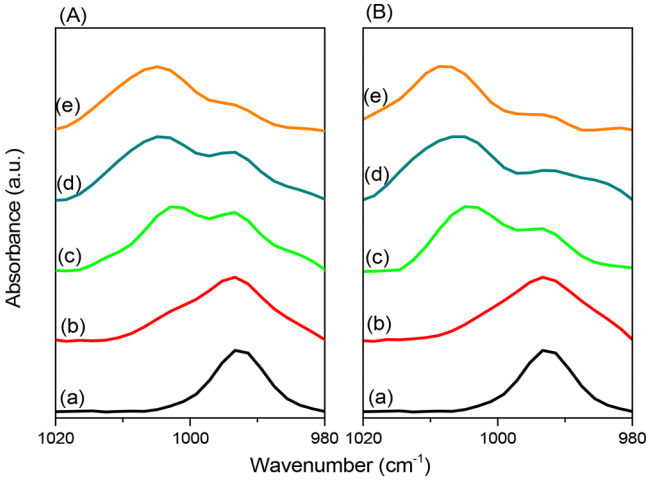

Figure 2. FTIR spectra (pyridine vibration region, 1020−980 cm^{-1}), recorded at room temperature, of (a) pure PS-*b*-P4VP and (b−e) PS-*b*-P4VP in the presence of the diblock copolymers (b) $PVPh_{20}$-*b*-$PMMA_{176}$, (c) $PVPh_{40}$-*b*-$PMMA_{112}$, (d) $PVPh_{137}$-*b*-$PMMA_{135}$, and (e) $PVPh_{137}$-*b*-$PMMA_{55}$ at (A) 30 and (B) 50 wt %.

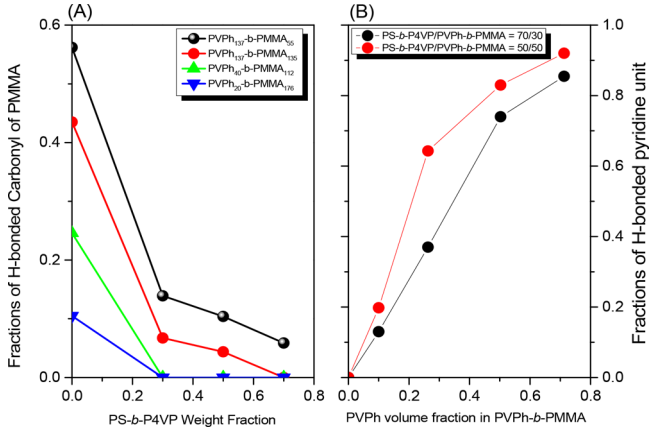

Figure 3. (A) Fractions of hydrogen-bonded C═O units in mixtures of PS-*b*-P4VP/PVPh-*b*-PMMA diblock copolymers upon increasing the concentration of the PS-*b*-P4VP diblock copolymer. (B) Fractions of hydrogen-bonded pyridine units in mixtures of PS-*b*-P4VP/PVPh-*b*-PMMA diblock copolymers upon increasing the PVPh volume fraction in the PVPh-*b*-PMMA diblock copolymers.

importantly, we know that the K_A value of PVPh/P4VP domain (K_A = 1200) is significantly higher than that of the PVPh-*b*-PMMA diblock copolymer (K_A = 47) as displayed in Table 2, and thus the fraction of hydrogen-bonded C═O units of PMMA decreased upon increasing the concentration of PS-*b*-P4VP in Figure 3A. This result implied that the OH units of PVPh would prefer to interact with the pyridine units of P4VP rather than the C═O units of PMMA, and thus the PMMA domain undergoes microphase separation from miscible PVPh-*b*-PMMA diblock copolymers and then induces the hierarchical self-assembled nanostructures.

Hierarchical Self-Assembled Nanostructures in PS-*b*-P4VP/PVPh-*b*-PMMA Diblock Copolymer Mixtures. Figure 4a presents the SAXS pattern of the pure PS-*b*-P4VP diblock copolymer (f_v^{PS} = 0.67), suggesting the long-range order of a bicontinuous gyroid structure having a peak ratio of $\sqrt{6}:\sqrt{8}:\sqrt{20}:\sqrt{26}:\sqrt{54}$, with the first peak appearing at a value of $\sqrt{6}q^*$ of 0.142 nm^{-1} (d = 44.22 nm). Figure 4f displays a corresponding TEM image confirming the presence of a bicontinuous gyroid structure from the [211] direction. At 30 wt % of the $PVPh_{137}$-*b*-$PMMA_{55}$ diblock copolymer, the SAXS pattern (Figure 4b) suggested a cylindrical structure having a peak ratio of $1:\sqrt{3}:\sqrt{4}$, as confirmed in the TEM image in Figure 4g. After staining with I_2 (causing the PS block

DOI: 10.1021/acs.macromol.8b00751
Macromolecules 2018, 51, 6451−6459

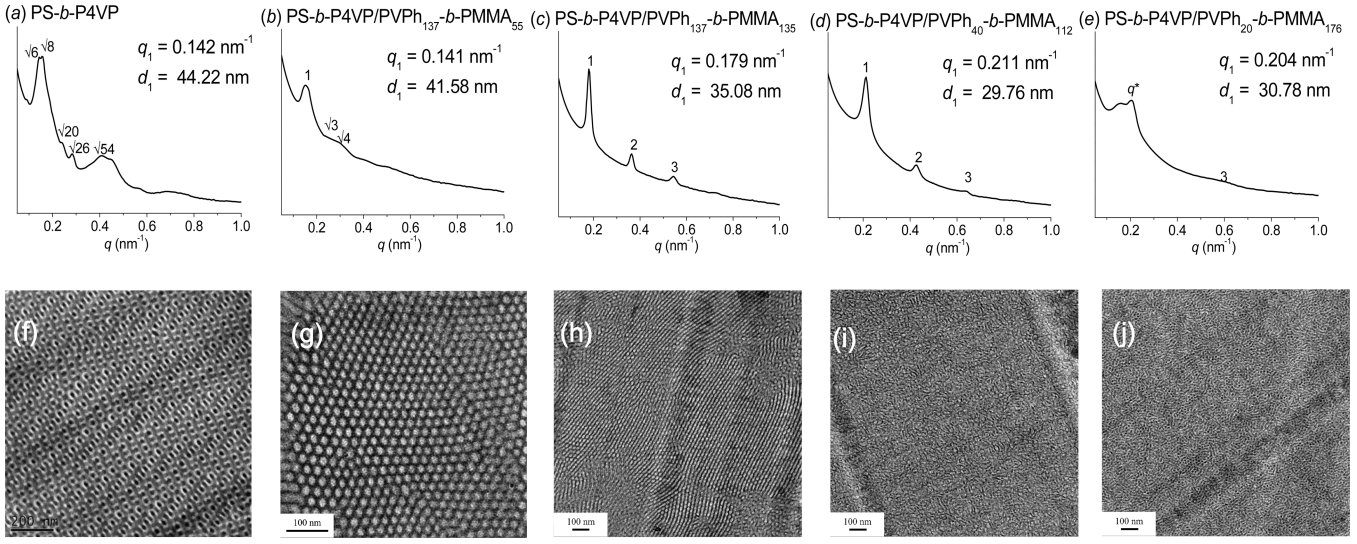

Figure 4. (a–e) SAXS and (f–j) TEM images of PS-*b*-P4VP/PVPh-*b*-PMMA = 70/30 diblock copolymer mixtures: (a, f) pure PS-*b*-P4VP, (b, g) $PVPh_{137}$-*b*-$PMMA_{55}$, (c, h) $PVPh_{137}$-*b*-$PMMA_{135}$, (d, i) $PVPh_{40}$-*b*-$PMMA_{112}$, and (e, j) $PVPh_{20}$-*b*-$PMMA_{176}$.

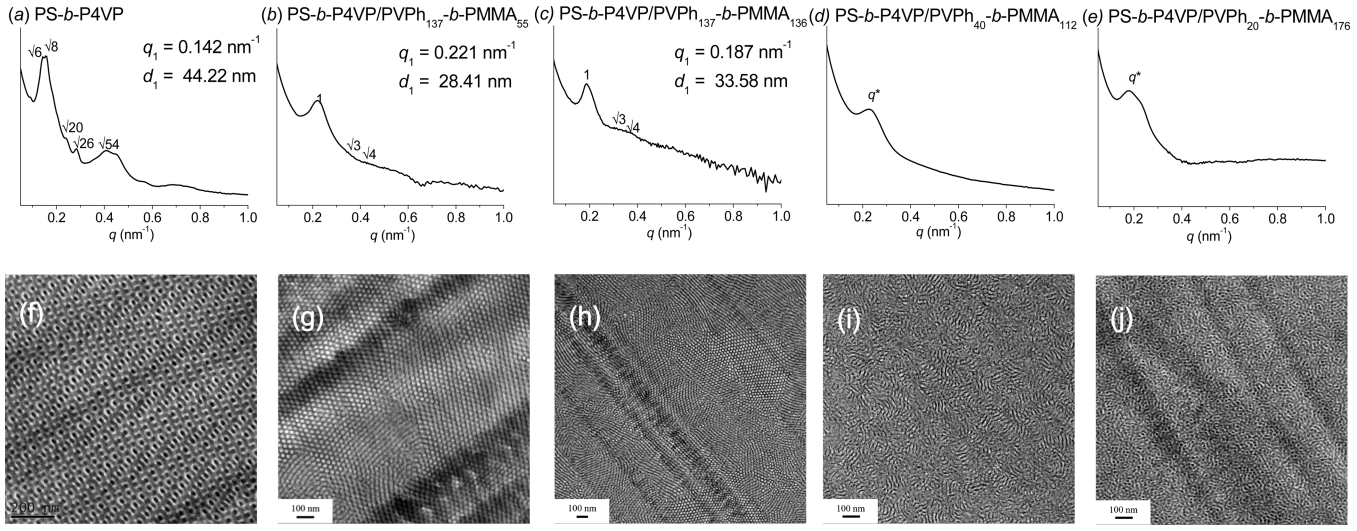

Figure 5. (a–e) SAXS and (f–j) TEM images of PS-*b*-P4VP/PVPh-*b*-PMMA = 50/50 diblock copolymer mixtures: (a, f) pure PS-*b*-P4VP, (b, g) $PVPh_{137}$-*b*-$PMMA_{55}$, (c, h) $PVPh_{137}$-*b*-$PMMA_{135}$, (d, i) $PVPh_{40}$-*b*-$PMMA_{112}$, and (e, j) $PVPh_{20}$-*b*-$PMMA_{176}$.

domains to appear as white regions and the P4VP-related domains as dark), the continuous phase of the PS domain was evident in Figure 4f, but it changed to the disperse phase of a cylindrical structure after blending with 30 wt % of the $PVPh_{137}$-*b*-$PMMA_{55}$ diblock copolymer (Figure 4g). Furthermore, in the presence of 30 wt % of the diblock copolymers $PVPh_{137}$-*b*-$PMMA_{135}$ and $PVPh_{40}$-*b*-$PMMA_{122}$, the SAXS patterns (Figures 4c and 4d, respectively) exhibited the long-range order of lamellar structures having peak ratios of 1:2:3, again confirmed through TEM imaging (Figures 4h and 4i, respectively). In addition, the SAXS pattern recorded in the presence of 30 wt % of the $PVPh_{20}$-*b*-$PMMA_{176}$ diblock copolymer (Figure 4e) displays the short-range order of a lamellar structure having a peak ratio of 1:3, as confirmed in the corresponding TEM image (Figure 4j). In addition, the *d*-spacing was generally decreased with the decreased of PVPh volume fraction in PVPh-*b*-PMMA diblock copolymer. Here, we observed that at the same ratio of the PVPh-*b*-PMMA diblock copolymer (30 wt %) and a similar volume fraction of PS block segments (f_v^{PS} = 0.537–0.522), the order–order morphological transition had already changed from a bicontinuous gyroid structure for the pure PS-*b*-P4VP diblock copolymer to a cylindrical structure for the $PVPh_{137}$-*b*-$PMMA_{55}$ diblock copolymer, but only to a lamellar structure for the other three PVPh-*b*-PMMA diblock copolymers. This phenomenon indicates that the effective interaction parameters had changed as a result of strong hydrogen bonding in the PVPh/P4VP complex; nevertheless, the different self-assembled structures were observed at similar volume fractions of the PS block segments due to the different fractions of hydrogen-bonded pyridine units of P4VP interacting with the different PVPh volumes fractions in the PVPh-*b*-PMMA diblock copolymers, as displayed in Figures 2 and 3. As a result, the degree of hydrogen bonding did indeed affect the self-assembled structures formed in the PS-*b*-P4VP/PVPh-*b*-PMMA diblock copolymer mixtures.

Figure 5 summarizes the SAXS patterns and TEM images of the PS-*b*-P4VP/PVPh-*b*-PMMA diblock copolymer mixtures incorporating 50 wt % of the PVPh-*b*-PMMA diblock copolymers. At 50 wt % of the diblock copolymer $PVPh_{137}$-

DOI: 10.1021/acs.macromol.8b00751
Macromolecules 2018, 51, 6451–6459

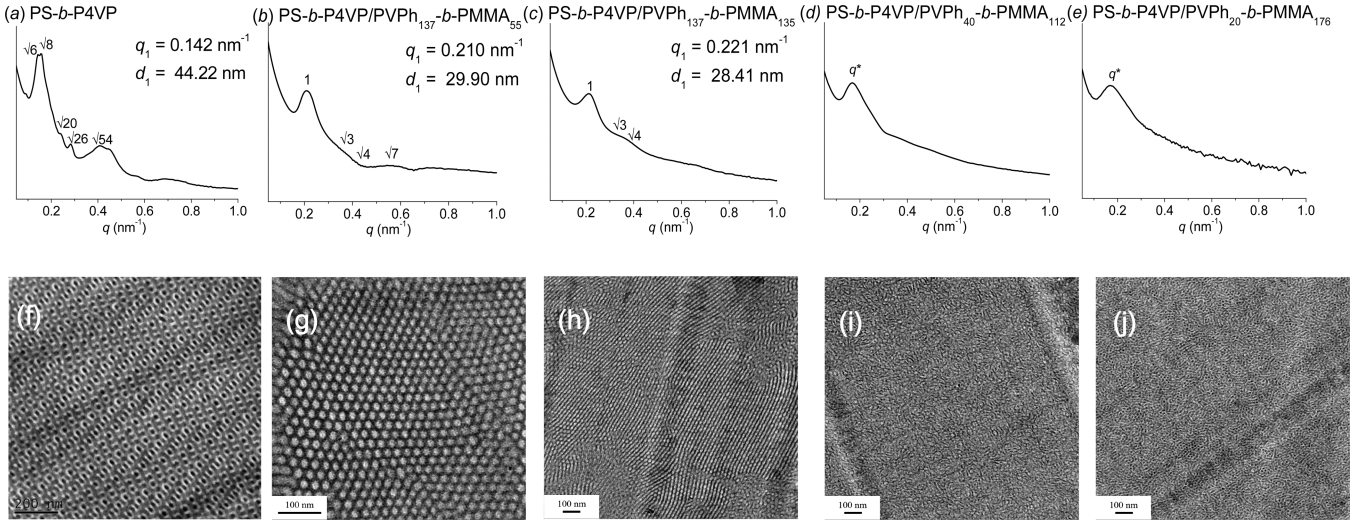

Figure 6. (a–e) SAXS and (f–j) TEM images of PS-*b*-P4VP/PVPh-*b*-PMMA = 30/70 diblock copolymer mixtures: (a, f) pure PS-*b*-P4VP, (b, g) $PVPh_{137}$-*b*-$PMMA_{55}$, (c, h) $PVPh_{137}$-*b*-$PMMA_{135}$, (d, i) $PVPh_{40}$-*b*-$PMMA_{112}$, and (e, j) $PVPh_{20}$-*b*-$PMMA_{176}$.

b-$PMMA_{55}$, the SAXS pattern (Figure 5b) again suggests a cylindrical structure having a peak ratio of $1:\sqrt{3}:\sqrt{4}$, as confirmed using TEM (Figure 5g), similar to that formed in the presence of 30 wt % of this diblock copolymer. Nevertheless, the *d*-spacing had decreased from 41.58 nm (30 wt %) to 28.41 nm (50 wt %) upon increasing the concentration of the $PVPh_{137}$-*b*-$PMMA_{55}$ diblock copolymer. This result indicates that the increase of the fraction of hydrogen-bonding interaction between the pyridine group of P4VP and the hydroxyl group of PVPh with the increase of PVPh-*b*-PMMA weight fraction as shown in Figure 3B. The strong hydrogen-bonding interaction may shrink the long period of P4VP segment. More interestingly, at 50 wt % of the diblock copolymer $PVPh_{137}$-*b*-$PMMA_{135}$, the SAXS pattern (Figure 5c) revealed a cylindrical structure having a peak ratio of $1:\sqrt{3}:\sqrt{4}$, as confirmed by the TEM image in Figure 5g; this structure is different from the lamellar structure formed in the presence of 30 wt % of this diblock copolymer. Thus, the order–order morphological transition could also occur from bicontinuous gyroid to lamellar to cylindrical structures upon increasing the content of the diblock copolymer $PVPh_{137}$-*b*-$PMMA_{135}$. Furthermore, at 50 wt % of the diblock copolymers $PVPh_{40}$-*b*-$PMMA_{122}$ and $PVPh_{20}$-*b*-$PMMA_{176}$, the SAXS patterns (Figures 5d and 5e, respectively) reveal the short-range order of only one broad peak, indicative of worm-like structures, which were confirmed in the TEM images in Figures 5i and 5j, respectively. Thus, lower PVPh volume fractions in the PVPh-*b*-PMMA diblock copolymers did not result in well-defined self-assembled structures due to relatively low fractions of hydrogen bonds with the pyridine units of the P4VP blocks.

Figure 6 presents the SAXS patterns and TEM images of the PS-*b*-P4VP/PVPh-*b*-PMMA diblock copolymer mixtures incorporating 70 wt % of the PVPh-*b*-PMMA diblock copolymers. At 70 wt % of the diblock copolymers $PVPh_{137}$-*b*-$PMMA_{55}$ and $PVPh_{137}$-*b*-$PMMA_{135}$, the SAXS patterns (Figures 6b and 6c, respectively) revealed the retention of cylindrical structures having peak ratios of $1:\sqrt{3}:\sqrt{4}$, as supported by the TEM images in Figures 6g and 6h, respectively; these structures are similar to those obtained in the presence of 50 wt % of these diblock copolymers. Furthermore, at 70 wt % of the diblock copolymers $PVPh_{40}$-*b*-$PMMA_{122}$ and $PVPh_{20}$-*b*-$PMMA_{176}$, the SAXS patterns (Figures 6d and 6e, respectively) revealed the short-range order of only one broad peak, indicative of worm-like structures, which were confirmed using TEM (Figures 6i and 6j, respectively).

Figure 7 displays the phase diagram of the PS-*b*-P4VP/PVPh-*b*-PMMA diblock copolymer mixtures. Here, we

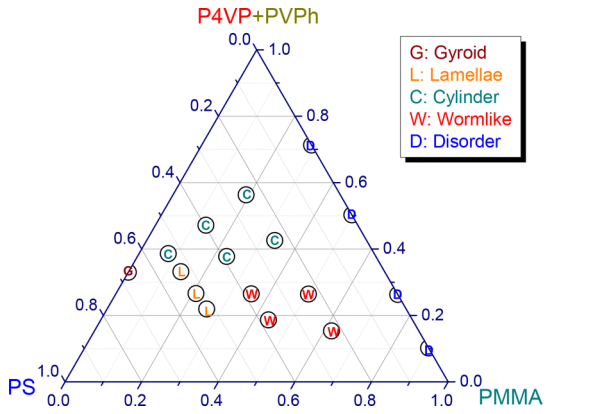

Figure 7. Phase diagram of mixtures of PS-*b*-P4VP and PVPh-*b*-PMMA diblock copolymers.

combined the PVPh/P4VP complex as one phase; we observe that higher PVPh/P4VP complex compositions formed cylindrical structures, higher PMMA compositions formed worm-like structures, and higher PS compositions formed lamellar structures. On the basis of this phase diagram, we could readily vary the self-assembled structures formed in these diblock copolymer mixtures. Note, however, that we had stained the samples only with I_2 and therefore could not observe the hierarchical self-assembly. We checked the DSC thermograms of PS-*b*-P4VP/$PVPh_{137}$-*b*-$PMMA_{135}$ = 50/50 diblock copolymer mixture (Figure 8). All other DSC thermograms of these diblock copolymer mixtures are displayed in Figure S1.

The pure PS-*b*-P4VP displayed two glass transition temperatures (T_g), at 104 and 154 °C, suggesting that the PS and P4VP block segments were phase-separated. In contrast, the

DOI: 10.1021/acs.macromol.8b00751
Macromolecules 2018, 51, 6451–6459

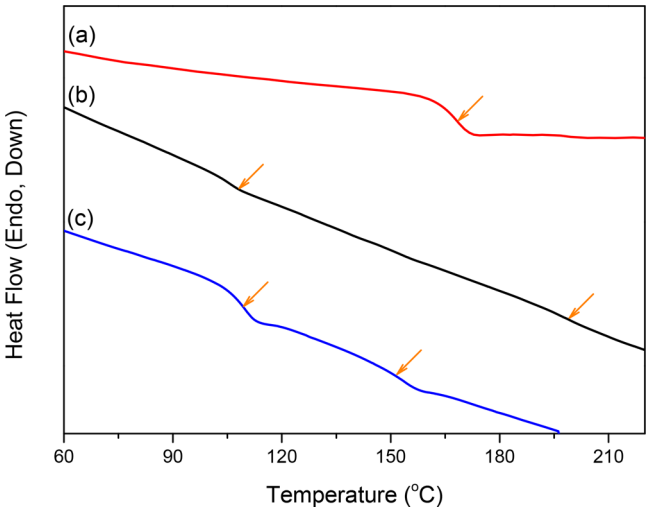

Figure 8. DSC thermograms of mixtures of (a) pure $PVPh_{137}$-*b*-$PMMA_{135}$, (b) PS-*b*-P4VP/$PVPh_{137}$-*b*-$PMMA_{135}$ = 50/50, and (c) pure PS-*b*-P4VP diblock copolymer.

diblock copolymer $PVPh_{137}$-*b*-$PMMA_{135}$ displayed only one value of T_g (at 168 °C), indicating that its PVPh and PMMA block segments were miscible as a result of hydrogen bonding. For the PS-*b*-P4VP/$PVPh_{137}$-*b*-$PMMA_{135}$ = 50/50 diblock copolymer mixture, we also observed two values of T_g (at 107 and 197 °C). The higher value of T_g corresponds to the PVPh/P4VP complex domain which is higher than those of individual homopolymers due to the featuring strong hydrogen bonding of these two block segments, and thus the volume fraction should change in this blend system. In addition, the lower value might be due to either the PS or PMMA segment because the glass transition temperature behaviors of pure PS and pure PMMA are similar. As a result, it was difficult to distinguish the three-phase behavior of these PS-*b*-P4VP/PVPh-*b*-PMMA diblock copolymer mixtures when using DSC analysis. Herein, we suppose that the volume fractions of these three phase-behaviors for PS, PVPh/P4VP, and PMMA domains are displayed in Figure 8. In addition, from the SAXS results as displayed in Figures 4–6, the scattering results would be very complicated in this PS-*b*-P4VP/PVPh-*b*-PMMA diblock copolymer mixture since the intensity of SAXS is dependent on the electron density difference between two phases as also summarized in Table 2, and thus it would have six electron density differences, which is similar to six different interaction parameters. Because the electron density difference is not high and hydrogen-bonding interaction was found between PVPh and PMMA, some q reflections are not obvious in this system, which is also due to the more than two self-assembly structure existing in this diblock copolymer mixture.

As a result, we stained the samples of the diblock copolymer mixtures with RuO_4 for further TEM analyses. The TEM images recorded after staining with I_2 revealed the P4VP block domains; further staining with RuO_4 would reveal the PVPh and PMMA block domains in these diblock copolymer mixtures. Figure 9 presents two selected TEM images recorded after only stained with RuO_4, only stained with I_2, and stained both I_2 and RuO_4. Clearly, only stained with RuO_4 or only stained with I_2 both display cylinder structure as displayed in Figures 9a and 9b, respectively; however, core–shell cylindrical structure is evident in Figure 9c for the PS-*b*-P4VP/$PVPh_{137}$-*b*-$PMMA_{55}$ = 70/30. The PVPh/P4VP complex domains appeared dark; the PMMA domains appeared gray because of hydrogen-bonding interactions with PVPh, and the PS domains appeared white, as displayed in Figure 9d. In addition, only the alternative lamellar structure was observed by only stained with RuO_4 or I_2 as displayed in Figures 9e and 9f, respectively. Similarly, the three-phase lamellar structure was evident in Figure 9g for PS-*b*-P4VP/$PVPh_{137}$-*b*-$PMMA_{135}$ = 70/30, and the scheme is displayed in Figure 9h. Other TEM images about three-phase behavior of PS-*b*-P4VP/$PVPh_{40}$-*b*-

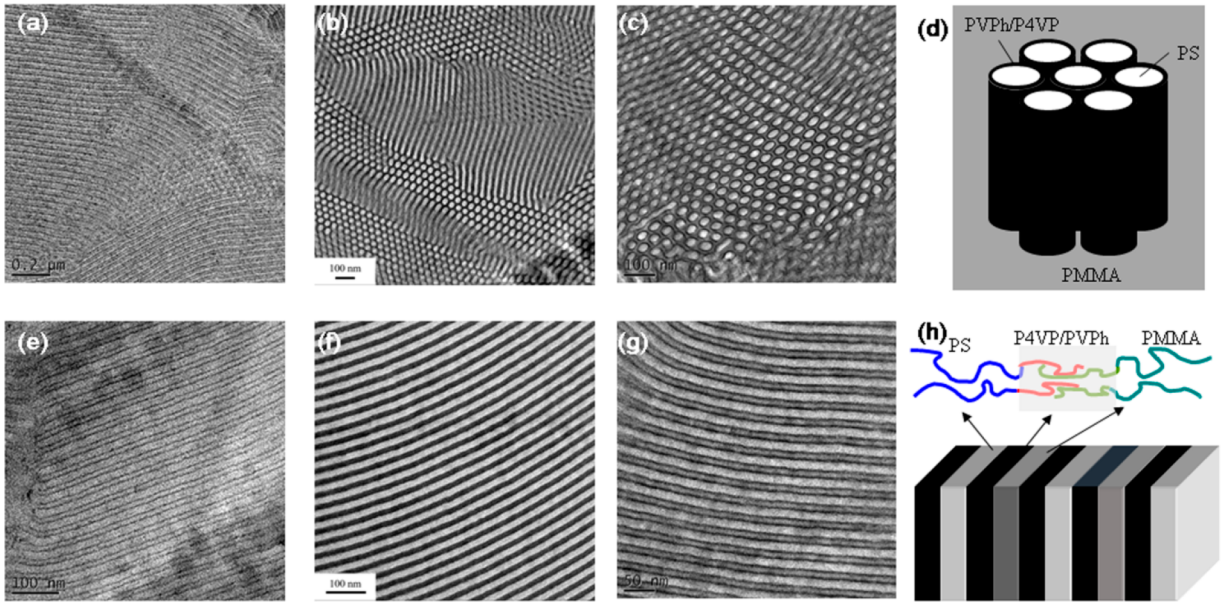

Figure 9. (a–c) TEM images of PS-*b*-P4VP/$PVPh_{137}$-*b*-$PMMA_{55}$ = 70/30 by (a) only stained RuO_4, (b) only stained I_2, (c) stained with both I_2 and RuO_4, and (d) schematic representation of the core–shell cylindrical structure. (e–g) TEM images of PS-*b*-P4VP/$PVPh_{137}$-*b*-$PMMA_{135}$ = 70/30 by (e) only stained RuO_4, (f) only stained I_2, (g) stained with both I_2 and RuO_4, and (h) schematic representation of three-phase lamellae, where the PVPh/P4VP complex domain appears dark, the PMMA domain appears gray, and the PS domain appears white.

DOI: 10.1021/acs.macromol.8b00751
Macromolecules 2018, 51, 6451–6459

$PMMA_{122}$ = 70/30, PS-*b*-P4VP/$PVPh_{20}$-*b*-$PMMA_{176}$ = 70/30, PS-*b*-P4VP/$PVPh_{137}$-*b*-$PMMA_{55}$ = 50/50, and PS-*b*-P4VP/$PVPh_{137}$-*b*-$PMMA_{135}$ = 50/50 both stained with RuO_4 or I_2 as displayed in Figure S2. Because the value of K_A of PVPh/P4VP is significantly larger than that for PVPh/PMMA, the fraction of hydrogen-bonded C═O units of PMMA would decrease strongly upon increasing the content of PS-*b*-P4VP. As a result, the PMMA block segments would be excluded from the miscible PVPh-*b*-PMMA diblock copolymer and, thereby, undergo microphase separation; because of the intrinsic immiscibility of PS and PMMA, mixtures of the PS-*b*-P4VP/PVPh-*b*-PMMA diblock copolymers will exist in three phases—PS, P4VP/PVPh, and PMMA domains—as displayed in Figures 9d and 9h. In addition, because the OH units of the PVPh blocks were confined in the PVPh/P4VP domain, the fraction of hydrogen-bonded pyridine units was increased; thus, these OH groups could not interact with the C═O units, and thus, the fraction of hydrogen-bonded C═O units of PMMA was significantly lower possibly because of the microphase-separated PMMA block segments and the OH units of PVPh strongly interacting instead with the pyridine units of the P4VP blocks. As a result, the PVPh and P4VP units are associated with hydrogen-bonding interaction; they naturally form the mixed one phase, and the phase behavior of PS and PMMA block segment becomes important in this study.

CONCLUSIONS

We have synthesized PS-*b*-P4VP and PVPh-*b*-PMMA diblock copolymers through sequential anionic living polymerizations. The fraction of hydrogen-bonded C═O units of the PMMA blocks decreases significantly upon increasing the concentration of PS-*b*-P4VP, based on FTIR spectroscopic analyses, because the value of K_A of PVPh/P4VP is significantly larger than that of PVPh/PMMA. As a result, the PMMA block segments were excluded from the miscible PVPh-*b*-PMMA diblock copolymer and underwent microphase separation; because of the intrinsic immiscibility of PS and PMMA, mixtures of the PS-*b*-P4VP/PVPh-*b*-PMMA diblock copolymers formed hierarchical self-assembled nanostructures, namely three-phase lamellar and core−shell cylindrical structures. This study is the first in which immiscible A-*b*-B diblock copolymers have been blended with disordered miscible C-*b*-D diblock copolymers, taking advantage of competitive hydrogen bonding and ΔK effects, to form hierarchical self-assembled nanostructures.

ASSOCIATED CONTENT

Supporting Information

The Supporting Information is available free of charge on the ACS Publications website at DOI: 10.1021/acs.macromol.8b00751.

Figures S1 and S2 (PDF)

AUTHOR INFORMATION

Corresponding Author

*E-mail: kuosw@faculty.nsysu.eu.tw (S.-W.K.).

ORCID

Shiao-Wei Kuo: 0000-0002-4306-7171

Notes

The authors declare no competing financial interest.

ACKNOWLEDGMENTS

This study was supported financially by the Ministry of Science and Technology, Taiwan, under Contracts MOST 106-2221-E-110-067-MY3 and 105-2221-E-110-092-MY3.

REFERENCES

(1) Jenekhe, S. A.; Chen, X. L. Self-assembly of ordered microporous materials from rod-coil block copolymers. *Science* **1999**, *283*, 372−375.

(2) Guiod, A. R.; Vandermeulen, W. M.; Klok, V. H. Advanced drug delivery devices via self-assembly of amphiphilic block copolymers. *Adv. Drug Delivery Rev.* **2012**, *64*, 270−279.

(3) Lin, E. L.; Hsu, W. L.; Chiang, Y. W. Trapping structural coloration by a bioinspired gyroid microstructure in solid state. *ACS Nano* **2018**, *12*, 485−493.

(4) Tang, J.; Liu, J.; Li, C.; Li, Y.; Tade, M. O.; Dai, S.; Yamauchi, Y. Synthesis of nitrogen-doped mesoporous carbon spheres with extra-large pores through assembly of diblock copolymer micelles. *Angew. Chem., Int. Ed.* **2014**, *54*, 588−593.

(5) Han, Y. K.; Pearce, E. M.; Kwei, T. K. Poly(styrene-b-vinylphenyldimethylsilanol) and its blends with homopolymers. *Macromolecules* **2000**, *33*, 1321−1329.

(6) Jiang, M.; Xie, H. Miscibility and morphology in block copolymer/homopolymer blends. *Prog. Polym. Sci.* **1991**, *16*, 977−1026.

(7) Zhao, J. Q.; Pearce, E. M.; Kwei, T. K. Binary and ternary blends of polystyrene-*block*-poly(*p*-hydroxystyrene). *Macromolecules* **1997**, *30*, 7119−7126.

(8) Kosonen, H.; Ruokolainen, J.; Nyholm, P.; Ikkala, O. Self-organized cross-linked phenolic thermosets: thermal and dynamic mechanical properties of novolac/block copolymer blends. *Polymer* **2001**, *42*, 9481−9486.

(9) Dobrosielska, K.; Wakao, S.; Takano, A.; Matsushita, Y. Nanophase-separated structures of AB block copolymer/C homopolymer blends with complementary hydrogen-bonding interactions. *Macromolecules* **2008**, *41*, 7695−7698.

(10) Dobrosielska, K.; Wakao, S.; Suzuki, J.; Noda, K.; Takano, A.; Matsushita, Y. Effect of homopolymer molecular weight on nanophase-separated structures of AB block copolymer/C homopolymer blends with hydrogen-bonding interactions. *Macromolecules* **2009**, *42*, 7098−7102.

(11) Chen, S. C.; Kuo, S. W.; Jeng, U. S.; Su, C. J.; Chang, F. C. On modulating the phase behavior of block copolymer/homopolymer blends via hydrogen bonding. *Macromolecules* **2010**, *43*, 1083−1092.

(12) Dehghan, A.; Shi, A. C. Modeling hydrogen bonding in diblock copolymer/homopolymer blends. *Macromolecules* **2013**, *46*, 5796−5805.

(13) Tsai, S. C.; Lin, Y. C.; Lin, E. L.; Chiang, Y. W.; Kuo, S. W. Hydrogen bonding strength effect on self-assembly supramolecular structures of diblock copolymer/homopolymer blends. *Polym. Chem.* **2016**, *7*, 2395−2409.

(14) Hameed, N.; Guo, Q. Nanostructure and hydrogen bonding in interpolyelectrolyte complexes of poly(ε-caprolactone)-*block*-poly(2-vinyl pyridine) and poly(acrylic acid). *Polymer* **2008**, *49*, 5268−5275.

(15) Hameed, N.; Liu, J.; Guo, Q. Self-assembled complexes of poly(4-vinylphenol) and poly(ε-caprolactone)-*block*-poly (2-vinylpyridine) via competitive hydrogen bonding. *Macromolecules* **2008**, *41*, 7596−7605.

(16) Hameed, N.; Guo, Q. Selective hydrogen bonding and hierarchical nanostructures in poly(hydroxyether of bisphenol A)/poly(ε-caprolactone)-*block*-poly(2-vinyl pyridine) blends. *Polymer* **2008**, *49*, 922−933.

(17) Chen, W. C.; Kuo, S. W.; Lu, C. H.; Jeng, U. S.; Chang, F. C. Self-assembly structures through competitive interactions of crystalline−amorphous diblock copolymer/homopolymer blends: Poly(ε-caprolactone-b-4-vinyl pyridine)/poly(vinyl phenol). *Macromolecules* **2009**, *42*, 3580−3590.

DOI: 10.1021/acs.macromol.8b00751
Macromolecules 2018, 51, 6451−6459

(18) Salim, N. V.; Hanley, T.; Guo, Q. Microphase separation through competitive hydrogen bonding in double crystalline diblock copolymer/homopolymer blends. *Macromolecules* **2010**, *43*, 7695−7704.
(19) Li, J. G.; Lin, Y. D.; Kuo, S. W. From microphase separation to self-organized mesoporous phenolic resin through competitive hydrogen bonding with double-crystalline diblock copolymers of poly(ethylene oxide-b-ε-caprolactone). *Macromolecules* **2011**, *44*, 9295−9309.
(20) Salim, N. V.; Hameed, N.; Guo, Q. Competitive hydrogen bonding and self-assembly in poly(2-vinyl pyridine)-*block*-poly-(methyl methacrylate)/poly(hydroxyether of bisphenol A) blends. *J. Polym. Sci., Part B: Polym. Phys.* **2009**, *47*, 1894−1905.
(21) Hameed, N.; Salim, N. V.; Guo, Q. Microphase separation through competitive hydrogen bonding in self-assembled diblock copolymer/homopolymer complexes. *J. Chem. Phys.* **2009**, *131*, 214905.
(22) Lee, H. F.; Kuo, S. W.; Huang, C. F.; Lu, J. S.; Chan, S. C.; Wang, C. F.; Chang, F. C. Hydrogen-bonding interactions mediate the phase behavior of an AB/C block copolymer/homopolymer blend comprising poly (methyl methacrylate-b-vinylpyrrolidone) and poly (vinylphenol). *Macromolecules* **2006**, *39*, 5458−5465.
(23) Chen, W. C.; Kuo, S. W.; Jeng, U. S.; Chang, F. C. Self-assembly through competitive interactions of miscible diblock copolymer/homopolymer blends: Poly (vinylphenol-b-methyl methacrylate)/poly (vinylpyrrolidone) blend. *Macromolecules* **2008**, *41*, 1401−1410.
(24) Zhou, J.; Shi, A. C. Microphase separation induced by differential interactions in diblock copolymer/homopolymer blends. *J. Chem. Phys.* **2009**, *130*, 234904.
(25) Lin, I.; Kuo, S. W.; Chang, F. C. Self-Assembly structures through competitive interactions of miscible crystalline−amorphous diblock copolymer/homopolymer blends. *Polymer* **2009**, *50*, 5276−5287.
(26) Matsushita, Y. Creation of hierarchically ordered nanophase structures in block polymers having various competing interactions. *Macromolecules* **2007**, *40*, 771−776.
(27) Miyase, H.; Asai, Y.; Takano, A.; Matsushita, Y. Kaleidoscopic tiling patterns with large unit cells from ABC star-shaped terpolymer/diblock copolymer blends with hydrogen bonding interaction. *Macromolecules* **2017**, *50*, 979−986.
(28) Asari, T.; Matsuo, S.; Takano, A.; Matsushita, Y. Three-phase hierarchical structures from AB/CD diblock copolymer blends with complemental hydrogen bonding interaction. *Macromolecules* **2005**, *38*, 8811−8815.
(29) Asari, T.; Arai, S.; Takano, A.; Matsushita, Y. Archimedean tiling structures from ABA/CD block copolymer blends having intermolecular association with hydrogen bonding. *Macromolecules* **2006**, *39*, 2232−2237.
(30) Kuo, S. W. Hydrogen bond-mediated self-assembly and supramolecular structures of diblock copolymer mixtures. *Polym. Int.* **2009**, *58*, 455−464.
(31) Chen, W. C.; Kuo, S. W.; Chang, F. C. Self-assembly of an A−B diblock copolymer blended with a C homopolymer and a C−D diblock copolymer through hydrogen bonding interaction. *Polymer* **2010**, *51*, 4176−4184.
(32) Kuo, S. W.; Tung, P. H.; Lai, C. L.; Jeong, K. U.; Chang, F. C. Supramolecular micellization of diblock copolymer mixtures mediated by hydrogen bonding for the observation of separated coil and chain aggregation in common solvents. *Macromol. Rapid Commun.* **2008**, *29*, 229−233.
(33) Kuo, S. W.; Tung, P. H.; Chang, F. C. Hydrogen bond mediated supramolecular micellization of diblock copolymer mixture in common solvents. *Eur. Polym. J.* **2009**, *45*, 1924−1935.
(34) Hsu, C. H.; Kuo, S. W.; Chen, J. K.; Ko, F. H.; Liao, C. S.; Chang, F. C. Self-assembly behavior of AB diblock and CD random copolymer mixtures in the solution state through mediated hydrogen bonding. *Langmuir* **2008**, *24*, 7727−7734.
(35) Tang, C.; Lennon, E. M.; Fredrickson, G. H.; Kramer, E. J.; Hawker, C. J. Evolution of block copolymer lithography to highly ordered square arrays. *Science* **2008**, *322*, 429−432.
(36) Lu, Y. S.; Kuo, S. W. Functional groups on POSS nanoparticles influence the self-assembled structures of diblock copolymer composites. *RSC Adv.* **2014**, *4*, 34849−34859.
(37) Lu, Y. S.; Yu, C. Y.; Lin, Y. C.; Kuo, S. W. Hydrogen bonding strength of diblock copolymers affects the self-assembled structures with octa-functionalized phenol POSS nanoparticles. *Soft Matter* **2016**, *12*, 2288−2300.
(38) Lin, C. L.; Chen, W. C.; Liao, C. S.; Su, Y. C.; Huang, C. F.; Kuo, S. W.; Chang, F. C. Sequence distribution and polydispersity index affect the hydrogen-bonding strength of poly (vinylphenol-co-methyl methacrylate) copolymers. *Macromolecules* **2005**, *38*, 6435−6444.
(39) Kuo, S. W.; Tung, P. H.; Chang, F. C. Syntheses and the study of strongly hydrogen-bonded poly (vinylphenol-b-vinylpyridine) diblock copolymer through anionic polymerization. *Macromolecules* **2006**, *39*, 9388−9395.
(40) Coleman, M. M.; Painter, P. C. *Miscible Polymer Blends: Background and Guide for Calculations and Design*; DEStech Publication Inc.: Lancaster, PA, 2006.
(41) Le Menestrel, C.; Bhagwagar, D. E.; Painter, P. C.; Coleman, M. M.; Graf, J. F. Hydrogen bonding in ternary polymer blend systems: determination of association parameters. *Macromolecules* **1992**, *25*, 7101−7106.
(42) Kuo, S. W.; Lin, C. L.; Chang, F. C. Phase behavior and hydrogen bonding in ternary polymer blends of phenolic resin/poly (ethylene oxide)/poly (ε-caprolactone). *Macromolecules* **2002**, *35*, 278−285.
(43) Huang, C. F.; Kuo, S. W.; Lin, F. J.; Huang, W. J.; Wang, C. F.; Chen, W. Y.; Chang, F. C. Influence of PMMA-chain-end tethered polyhedral oligomeric silsesquioxanes on the miscibility and specific interaction with phenolic blends. *Macromolecules* **2006**, *39*, 300−308.

DOI: 10.1021/acs.macromol.8b00751
Macromolecules 2018, 51, 6451−6459